Misfolded proteinase K–resistant hyperphosphorylated α-synuclein in aged transgenic mice with locomotor deterioration and in human α-synucleinopathies

Manuela Neumann,[1] Philipp J. Kahle,[2] Benoit I. Giasson,[3] Laurence Ozmen,[4] Edilio Borroni,[4] Will Spooren,[4] Veronika Müller,[2] Sabine Odoy,[2] Hideo Fujiwara,[5] Masato Hasegawa,[5] Takeshi Iwatsubo,[5] John Q. Trojanowski,[3] Hans A. Kretzschmar,[1] and Christian Haass[2]

[1]Department of Neuropathology, and
[2]Laboratory for Alzheimer's and Parkinson's Disease Research, Department of Biochemistry, Ludwig Maximilians University, Munich, Germany
[3]Department of Pathology and Laboratory Medicine, University of Pennsylvania, School of Medicine, Philadelphia, Pennsylvania, USA
[4]Pharma Research, F. Hoffmann–La Roche Ltd., Basel, Switzerland
[5]Department of Neuropathology and Neuroscience, Graduate School of Pharmaceutical Sciences, University of Tokyo, Tokyo, Japan

The pathological modifications of α-synuclein (αS) in Parkinson disease and related diseases are poorly understood. We have detected misfolded αS in situ based on the proteinase K resistance (PK resistance) of αS fibrils, and using specific antibodies against S129-phosphorylated αS as well as oxidized αS. Unexpectedly massive neuritic pathology was found in affected human brain regions, in addition to classical αS pathology. PK resistance and abnormal phosphorylation of αS developed with increasing age in (Thy1)-h[A30P] αS transgenic mice, concomitant with formation of argyrophilic, thioflavin S-positive, and electron-dense inclusions that were occasionally ubiquitinated. αS pathology in the transgenic mice was predominantly in the brainstem and spinal cord. Astrogliosis was found in these heavily affected tissues. Homozygous mice showed the same pathology approximately one year earlier. The transgenic mice showed a progressive deterioration of locomotor function. Thus, misfolding and hyperphosphorylation of αS may cause dysfunction of affected brain regions.

Introduction

The presynaptic protein α-synuclein (αS) is genetically and pathologically linked to a variety of neurodegenerative diseases (1). Disruption of αS gene expression in mice (2) and primary neurons (3) suggested that αS is implicated in dopaminergic (DA) neurotransmission.

Two missense mutations in the αS gene cause autosomal-dominant hereditary Parkinson disease (PD) (4, 5). Moreover, αS fibrils are the major component of Lewy bodies (LBs) and Lewy neurites (LNs), the hallmark lesions in PD, dementia with LBs (DLB), LB variant of Alzheimer disease, neurodegeneration with brain iron accumulation type 1 (NBIA1; formerly known as Hallervorden-Spatz disease), and pure autonomic failure (6–9). In addition to such neuronal Lewy pathology, glial cytoplasmic inclusions composed of αS fibrils occur in multiple system atrophy (MSA) (10).

Phosphorylation of αS at S129 (11) is a specific marker of α-synucleinopathy lesions (12). S129 phosphorylation enhances the propensity of αS to form fibrils in vitro (12), comparable to the effect of PD-associated mutations and oxidative stress (13–16). αS fibrils are also resistant to limited digestion with proteinase K (PK) (17–19), similar to aggregates formed by proteins relevant to other neurodegenerative diseases, such as prion protein (PrP) and amyloid β-protein (20). In contrast, the nonamyloidogenic βS

was PK-sensitive, probably due to lack of a critical stretch of amino acids in the NAC domain (18).

Several animal models have been developed based on transgenic expression of αS. Transgenic expression of αS in *Drosophila* caused LB pathology and age-dependent DA neuron loss, which could be ameliorated by coexpression of the molecular chaperone Hsp70 (21, 22). Expression of αS in transgenic mouse neurons partially reproduced some features of human Lewy pathology, namely accumulation of detergent-insoluble αS in neuronal cell bodies and swollen neurites (23–26). Ubiquitination was occasionally observed (23, 24), and a modest reduction in DA markers was reported for one mouse model (23). This was enhanced upon crossbreeding with mice expressing mutant amyloid precursor protein (27), and ameliorated by coexpression of the antiamyloidogenic synuclein homolog βS (28).

The relatively high prevalence of PD in the elderly (29) implies that aging is a risk factor of α-synucleinopathy. Here we report that in aged (Thy1)-h[A30P]αS mice a considerable portion of transgenic αS turned PK-resistant, whereas the nonamyloidogenic βS was completely digested with PK under the same conditions, accurately reflecting the human pathology. Misfolding of αS in neurites was further corroborated with a variety of specific antibodies. The formation of PK-resistant αS in aged transgenic mice coincided with the appearance of argyrophilic, thioflavin S–positive (TS-positive), and electron-dense inclusions, some of which were labeled with antibodies against ubiquitin. Moreover, pathological profiles in the aged transgenic mice displayed the diagnostic S129 hyperphosphorylation. Homozygous mice developed the same pathology at least 1 year earlier than heterozygotes and showed a progressive deterioration of locomotor function. Thus, we present a mouse model that recapitulates cardinal features of PD pathology including PK resistance, which we demonstrate here to provide a highly sensitive method to detect pathologically misfolded αS.

Methods

Antibodies. Rat monoclonal anti-αS 15G7 hybridoma supernatant, mouse monoclonal MC42 against synuclein-1 (Transduction Laboratories, Lexington, Kentucky, USA), rabbit polyclonal anti-αS antiserum 3400 (Affiniti Research Products Ltd., Mamhead, United Kingdom), rabbit polyclonal anti-βS antiserum 6485, and rabbit polyclonal antiserum against phospho-αS (12) were used as described previously (25). Mouse monoclonal antibodies Syn303 and Syn514 were raised against oxidized αS (30). Antisera against ubiquitin (working dilution 1:300) and glial fibrillary acidic protein (working dilution 1:500) were purchased from DAKO A/S (Glostrup, Denmark). Peroxidase-conjugated anti-mouse IgG and anti-rabbit IgG (working dilution 1:5,000) were purchased from Sigma-Aldrich (St. Louis, Missouri, USA). Goat anti-rat IgG–peroxidase conjugate (working dilution 1:1,000) was purchased from Santa Cruz Biotechnology Inc. (Santa Cruz, California, USA).

Aggregation and phosphorylation of synucleins in vitro. Human [wt]αS, [Δ73-83]αS, and [wt]βS, and mouse [wt]αS were expressed and purified as described previously (26). Protein solutions were reconstituted from lyophilized stocks and precleared by ultracentrifugation. Aggregation mixes in 50 mM PBS (pH 7) were incubated at 37°C with constant agitation. Aliquots were taken at the indicated times and digested with PK (QIAGEN GmbH, Hilden, Germany) for 30 minutes at 37°C. The resulting Western blots were scanned, and band intensities were quantified using NIH Image version 1.62 freeware (available at http://rsb.info.nih.gov/nih-image).

Five units of casein kinase 1 (New England Biolabs Inc., Frankfurt, Germany) were used per nanogram freshly dissolved synuclein in phosphorylation reactions, as described previously (11).

PK digestion of human brain extracts. Approximately 1 g of tissue was homogenized in buffer A (1 mM dithiothreitol; 1 mM EGTA; 50 mM Tris, pH 7.5) and extracted as described previously (19). Briefly, the buffer-insoluble 350,000-*g* pellet was resuspended in 1% Triton X-100. The Triton-insoluble 350,000-*g* pellet was resuspended in 0.5 M NaCl/10% sucrose. After 350,000 *g* centrifugation, the pellet was resuspended in 0.5 M NaCl/10% sucrose plus 1% sarcosyl and incubated for 1 hour at 37°C. The extract was cleared by 20 minutes' centrifugation at 27,000 *g*. PK was added to the supernatant and incubated for 30 minutes at 37°C. The reactions were stopped by addition of SDS-PAGE loading buffer.

PK-digested paraffin-embedded tissue blots. The PK-digested paraffin-embedded tissue (PK-PET) blot was performed as described previously (31) with minor modifications. Briefly, 5-μm sections from paraffin-embedded tissue were cut on a microtome, placed in a water bath (55°C), collected on a wet 0.45-μm nitrocellulose membrane (Bio-Rad Laboratories Inc., Richmond, California, USA), and dried for at least 8 hours at 55°C. The section on the nitrocellulose membrane was deparaffinized with xylene and rehydrated using a descending ethanol series. After wetting with TBS-T (10 mM Tris-HCl, pH 7.8; 100 mM NaCl; 0.05% Tween-20), digestion was performed with 50 μg/ml PK (Roche Molecular Biochemicals, Mannheim, Germany) in TBS-B (10 mM Tris-HCl, pH 7.8; 100 mM NaCl; 0.1% Brij-35) for 8–14 hours at 55°C. After washing 3 times with TBS-T, the proteins on the membranes were denatured with 3 M guanidine isothiocyanate in 10 mM Tris-HCl (pH 7.8) for 10 minutes. After preincubation in blocking solution (0.2% casein in TBS-T) for 30 minutes, immunostaining was performed with monoclonal 15G7 anti-αS (dilution 1:50) or polyclonal 6485 anti-βS (dilution 1:200) for 8 hours at 4°C. After three washes in TBS-T, incubation for at least 1 hour was performed with an alkaline phosphatase–coupled goat anti-rabbit antibody (dilution 1:500; DAKO A/S). In the case of 15G7, incubation with a bridging rabbit anti-rat antibody (dilution 1:500) was performed for 1 hour. After five washes in TBS-T for 10 minutes, the membranes were adjusted to alkaline pH by incubation

two times for 5 minutes in NTM (100 mM Tris-HCl, pH 9.5; 100 mM NaCl; 50 mM MgCl$_2$). The visualization of the antibody reaction was provided by formazan reaction using nitrotetrazolium blue/5-bromo-4-chloro-3-indolyl phosphate p-toluidine salt. Blots were evaluated with a dissecting microscope (Olympus Optical GmbH, Hamburg, Germany).

Generation of homozygous (Thy1)-h[A30P]αS transgenic mice. Heterozygous line 31 (Thy1)-h[A30P]αS mice (25) were backcrossed over eight generations into the C57BL/6J strain (RCC Ltd., Füllinsdorf, Switzerland), and intercrossed to produce line 31H, which is homozygous for the transgene. The genetic background of these mice was distinct from the so-called C57BL/6S substrain harboring a spontaneous deletion of the αS locus (32), since endogenous mouse αS was detectable in the (Thy1)-h[A30P]αS transgenics (26).

Histological and immunohistochemical analysis of brains from transgenic mice and human patients. Brain and spinal cord (SC) from transgenic mice and patients with human α-synucleinopathies (PD, DLB, NBIA1, MSA) were fixed in 4% formalin in PBS and embedded in paraffin. Sections (4 µm) were examined with hematoxylin and eosin, Nissl, Gallyas silver, Campbell-Switzer silver, and TS stains. To enhance immunoreactivity for αS, sections were either boiled in 0.01 M citrate buffer (pH 6.0) five times for 3 minutes, or pretreated with PK (100 µg/ml; Roche Molecular Biochemicals) in 50 mM Tris-HCl buffer (pH 7.4) containing 5 mM EDTA for 10 minutes at 37°C, or 99% formic acid (Sigma-Aldrich) for 10 minutes at room temperature. Antibody binding was detected using the alkaline phosphatase/anti–alkaline phosphatase system (DAKO A/S) or the avidin-biotin complex system (Vector Laboratories Inc., Burlingame, California, USA).

Electron microscopy. Formalin-fixed brain tissue from transgenic mice was fixed in 3% buffered glutaraldehyde, post-fixed in 1% osmium tetroxide, dehydrated, and embedded in araldite. Ultrathin sections were contrasted with lead citrate, and examination was performed using a Zeiss EM 10 microscope (Carl Zeiss, Oberkochen, Germany).

Tissue levels of monoamines. Mice were sacrificed by decapitation. The brains were quickly removed from the skull, briefly washed in ice-cold saline, and laid on a cooled (4°C) metal plate, where they were rapidly dissected to remove the striatum and frontal cortex. The dissected brain regions were frozen, weighed, and stored at –80°C until analysis. The contents of monoamines and their metabolites were determined using an HPLC system equipped with an electrochemical detector (Coulochem II detector, model 5200; ESA Inc., Chelmsford, Massachusetts, USA) essentially as described (33). Briefly, the striata and frontal cortices were homogenized with an ultrasonic processor in 0.1 M perchloric acid containing 0.5 mM disodium EDTA and 50 ng/ml 3,4-dihydroxybenzylamine as an internal standard.

The homogenates were centrifuged at 51,000 *g*, and 5 µl of the supernatant was injected in the HPLC. Monoamines and their metabolites were separated on a reverse-phase ODS column (YMC-Pack, S-3 µM, 120 A; Stagroma AG, Reinach, Switzerland). The column temperature was maintained at 33°C. The mobile phase was 34% citric acid 0.1 M, 48% Na$_2$HPO$_4$ 0.1 M, 18% methanol, 50 mg/l EDTA, and 45 mg/l sodium octylsulfate, pH 4.5. The flow rate was set at 0.45 ml/min. The potential settings of the analytical cell
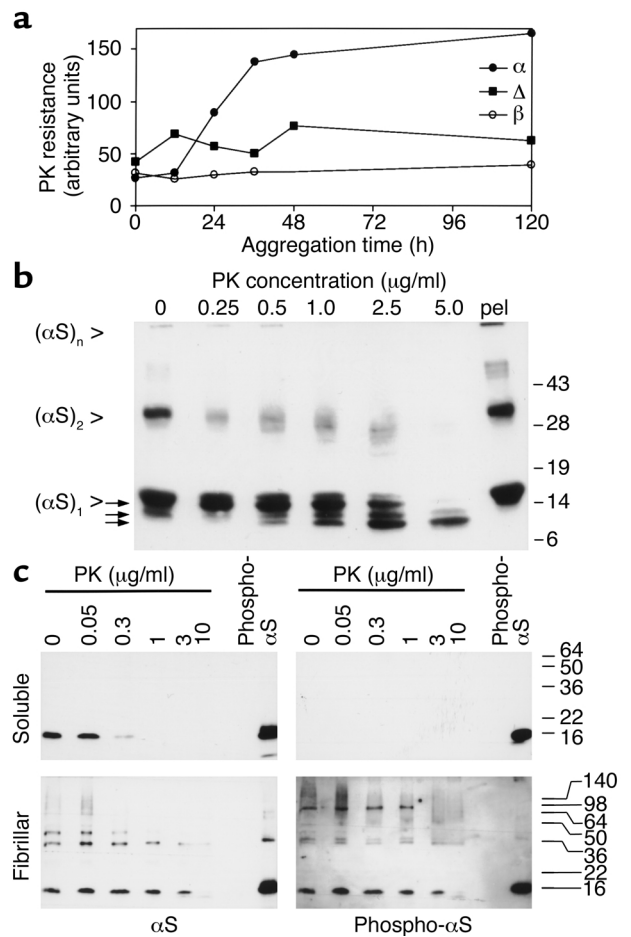

Figure 1

αS becomes PK-resistant upon aggregation in vitro. (**a**) Two milligrams per milliliter [wt]αS (filled circles), [Δ73-83]αS (filled squares), and [wt]βS (open circles) were incubated for the indicated times, at which 5-µl samples were taken and treated with PK. Western blots were probed with MC42 to detect [wt]αS and [Δ73-83]αS, and antiserum 6485 to detect [wt]βS. Band signals were quantitated by densitometric scanning. (**b**) Two milligrams per milliliter [wt]αS were aggregated for 7 days, then digested with the indicated amount of PK, or pelleted by ultracentrifugation (pel). Arrows point to fragments liberated from full-length αS (see text for details). Western blot was probed with 3400 anti-αS. (**c**) Tissue from a DLB patient was extracted, and the soluble (upper panels) and fibril-containing (lower panels) fractions were digested with the indicated concentrations of PK. Western blots were sequentially probed with phosphospecific anti-αS (right panels) and 15G7 anti-αS (left panels). Exposure times of the blots were chosen to match the intensities of the standard bands (20 ng in vitro–phosphorylated recombinant αS). The experiments were repeated with the same results.
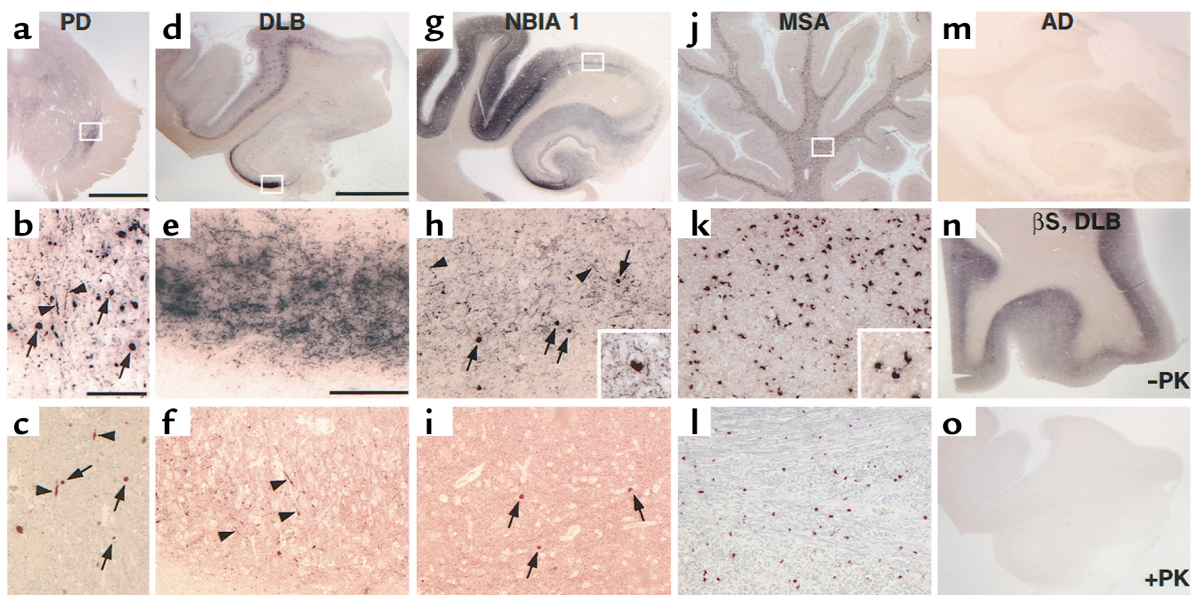
Figure 2

PK-PET blots and immunohistochemistry in human α-synucleinopathies. (**a–l**) Representative brain sections from (**a–c**) PD, (**d–f**) DLB, (**g–i**) NBIA1, and (**j–l**) MSA patients. PK-resistant αS was found on PK-PET blots of PD SN (**a**) as well as hippocampus and temporal cortex in DLB (**d**) and NBIA1 (**g**) brains. (**b, e,** and **h**) Higher magnification of the regions boxed in **a**, **d**, and **g**, respectively, shows several LBs (arrows; inset in **h**), as does standard anti-αS immunohistochemistry of adjacent sections (**c, f,** and **i**). In contrast, many more LNs (arrowheads) were observed on PK-PET blots (**b, e,** and **h**) than on standard sections (**c, f,** and **i**). (**j**) PK-resistant αS was also detected in cerebellar white matter of MSA patients. (**k**) Higher magnification of the area boxed in **j** demonstrates PK-resistant αS in glial cytoplasmic inclusions (inset in **k**), as confirmed by standard αS immunohistochemistry of an adjacent section (**l**). (**m**) No staining was noted on PK-PET blots in the hippocampal formation of Alzheimer disease (AD) patients. (**n** and **o**) Antibody against βS in a DLB case shows an intense staining only without PK digest (**n**), whereas virtually no staining remained after PK treatment (**o**). Scale bar in **a**, 5 mm; in **b**, 200 μm (**b** and **c**); in **d**, 5 mm (**d, g, j,** and **m–o**); in **e**, 200 μm (**e, f, h, i, k,** and **l**).

(model 5011; ESA Inc.) were +0.45 V (first electrode) and –0.3 V (second electrode). Monoamines and their metabolites were read as second-electrode output signal.

Results

Formation of PK-resistant αS aggregates in vitro. αS formed PK-resistant aggregates in a time- and concentration-dependent manner. After 12 hours the first PK-resistant αS became detectable, and it continued to accrue until a plateau was reached after 36 hours (Figure 1a). Parallel incubations of the nonamyloidogenic βS did not produce any PK-resistant material, and the aggregation-deficient deletion mutant [Δ73-83]αS (26) had a greatly reduced capacity to form PK-resistant aggregates (Figure 1a). Diluting the αS below a critical concentration of 2 mg/ml completely prevented the formation of PK-resistant aggregates under these conditions (results not shown).

αS aggregates treated with PK yielded a characteristic cleavage pattern. From the 16-kDa αS monomer, three fragments of approximately 14 kDa, 12 kDa, and 10 kDa were generated with increasing PK concentrations (Figure 1b). The 14-kDa species was already visible at 0.25 μg/ml PK and disappeared along with the full-length band above 2.5 μg/ml PK. The 12-kDa and the more prominent 10-kDa species became detectable at 0.5 μg/ml PK and persisted to 5 μg/ml PK. The fragments were N-terminally truncated products, because the bands were detected with αS antibodies against C-terminal epitopes. Beyond 10 μg/ml PK, these proteolytic products were C-terminally processed to core NAC fragments (results not shown), consistent with previous reports (18, 19). Interestingly, the SDS-stable putative dimer bands around 30 kDa [(αS)₂], as well as aggregates that did not enter the separating gel [(αS)ₙ], were not particularly resistant to PK (Figure 1b).

PK-resistant αS detected in human α-synucleinopathies. To evaluate the PK resistance of αS in human brain, the tissue was fractionated (19). αS present in the buffer-soluble fraction was fully degraded with 1 μg/ml PK (Figure 1c). In contrast, the αS in the fraction enriched in fibrils was resistant to 1 μg/ml PK (Figure 1c). Even at 10 μg/ml, the cleavage was only half-maximal (Figure 1c). In control experiments we verified that the sarcosyl buffer components did not interfere with PK activity to that extent (data not shown). Thus, like in vitro–aggregated αS, the fibrillar αS extracted from human LB disease patients is more than ten times more resistant to PK than is the "healthy," soluble αS. As for in vitro aggregates, putative αS dimers in the fibrillar fractions were not particularly resistant to PK (Figure 1c).

Immunoreactivity with phosphospecific anti-αS was recently recognized as a pathological hallmark of α-synucleinopathy lesions (12). Thus, we examined the solubility and PK resistance of hyperphosphorylated αS. An antibody that reacts exclusively with αS

phosphorylated at S129 (12) detected bands only in the fibrillar fraction (Figure 1c). Both monomeric and oligomeric hyperphosphorylated αS species were observed in the fibrillar fraction (Figure 1c). The hyperphosphorylated αS in the fibrillar fraction was also found to be more than ten times more resistant to PK than the soluble, unphosphorylated αS (Figure 1c).

The PK resistance of αS aggregates prompted us to develop a novel histological method (PK-PET blot) to selectively detect pathological αS in situ, analogous to the detection of misfolded PrP (31, 34). Postmortem brain sections from patients with PD (*n* = 4), DLB (*n* = 5), NBIA1 (*n* = 1), MSA (*n* = 2), or Alzheimer disease (*n* = 2), and controls (*n* = 2), were blotted onto nitrocellulose membranes and subjected to PK digestion before immunodetection of αS. Thereby the abundant physiological PK-labile αS was removed, and PK-resistant pathological αS was unveiled in brain regions selectively affected by α-synucleinopathy. Brains from patients with LB diseases or MSA were examined (Figure 2).

Intense PK-PET blot labeling of αS was seen in PD striatum (not shown) and in the substantia nigra (SN) pars compacta of PD (Figure 2a), DLB, and NBIA1 brains (not shown). In PD and DLB cases with a limbic and neocortical subtype of LB pathology according to consensus criteria (35), PK-PET blots were strongly labeled with anti-αS in the hippocampus, particularly in the CA2/3 sector, and in the parahippocampal gyrus and temporal cortex, especially in deeper cortical layers (Figure 2d). PK-PET blot reactivity of anti-αS was particularly pronounced in an NBIA1 patient with severe cortical LB pathology (36). In this case, PK-PET blot signal of αS was found throughout the hippocampal formation, again concentrated in the CA2/3 sector, and was widespread in the temporal cortex (Figure 2g). Non-neuronal α-synucleinopathy was also visualized on PK-PET blots from MSA cerebellar white matter (Figure 2j). In contrast, no PK-resistant αS was detectable in pure Alzheimer disease cases (Figure 2m) and in control cases (data not shown). Likewise, the widely distributed, nonamyloidogenic βS was fully degraded after PK digest (Figure 2, n and o), as predicted from the in vitro experiments above.

Higher magnification of PK-PET blots showed the fine structure of PK-resistant αS inclusions. Both brainstem-type LBs (Figure 2b) and cortical LBs (Figure 2h) were visualized on PK-PET blots as expected from standard αS immunohistochemistry (Figure 2, c and i). Likewise, glial cytoplasmic inclusions were highlighted with anti-αS on PK-PET blots as they were on αS immunostained sections (Figure 2, k and l). Thus,
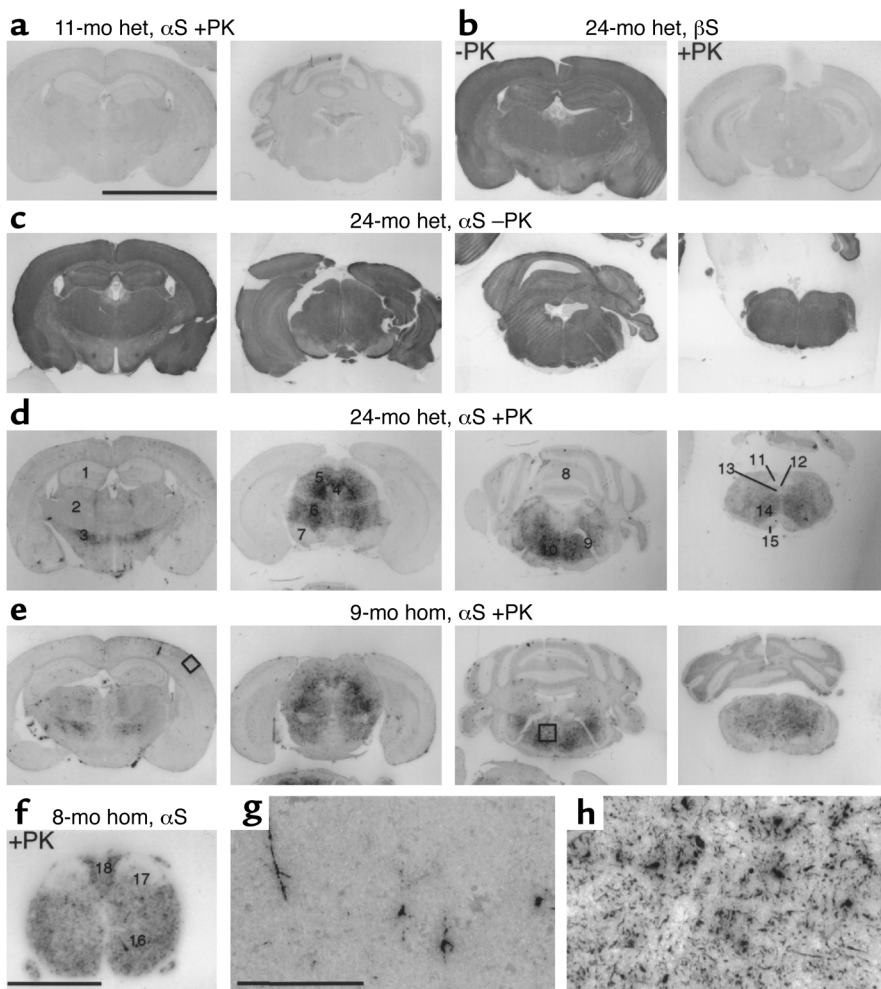

a 11-mo het, αS +PK

b 24-mo het, βS
−PK   +PK

c 24-mo het, αS −PK

d 24-mo het, αS +PK

e 9-mo hom, αS +PK

f 8-mo hom, αS +PK

g

h

Figure 3
Age-dependent formation of PK-resistant αS in transgenic mice. (**a**) αS PK-PET blots of an 11-month-old heterozygous (het) mouse showed no PK-resistant αS. (**b**) βS PK-PET blots of a 24-month-old heterozygous mouse showed no PK-resistant βS (+PK) despite strong staining of PK-labile βS (−PK). (**c** and **d**) PK-PET blots of a 24-month-old heterozygous mouse before (**c**) and after (**d**) PK treatment showed specific staining of PK-resistant αS only in specific brain regions, although transgenic αS was expressed throughout the brain. (**e**) The same pathology was already seen on αS PK-PET blots of a 9-month-old homozygous (hom) mouse. (**f**) αS PK-PET blot of the SC of an 8-month-old homozygous mouse. (**g** and **h**) Higher magnifications of the areas boxed in **e**, namely cortex (**g**) and pontine reticular field (**h**). Scale bar in **a**, 5 mm (**a**–**e**); in **f**, 1 mm; in **g**, 200 μm (**g** and **h**). Numbers in **d** and **f**: 1, hippocampus; 2, thalamus; 3, zona incerta; 4, aqueduct and periaqueductal gray; 5, superior colliculus; 6, mesencephalic nucleus; 7, SN; 8, cerebellum; 9, facial nerve root; 10, pontine zona reticulata; 11, nucleus of solitary tract; 12, aqueduct; 13, hypoglossal nucleus; 14, medullary zona reticulata; 15, pyramidal tract; 16, ventral horn; 17, dorsal horn; 18, dorsal columns.
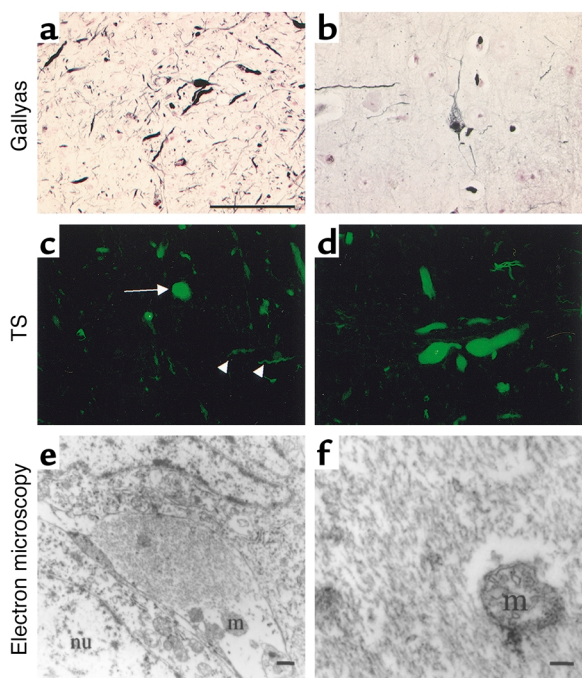
Figure 4
"Amyloid" pathology in aged transgenic mice. (**a** and **b**) Gallyas silver stain revealed numerous argyrophilic dystrophic neurites and some inclusions in cell bodies in the pontine reticular field (**a**) and the motor cortex (**b**) of a 9-month-old homozygous mouse. (**c** and **d**) TS stained numerous LB-like cytoplasmic inclusions (arrow in **c**) and dystrophic neurites (arrowheads in **c**), some of which were hugely inflated (**d**). (**e** and **f**) Transmission electron microscopy showing a spherical inclusion composed of the typical 9- to 12-nm straight filaments within a swollen neurite. m, mitochondria; nu, nucleus. Scale bar in **a** corresponds to 100 μm in **a** and 50 μm in **b**–**d**. Scale bar in **e**, 400 nm; in **f**, 125 nm.

the classical α-synucleinopathy lesions were reproducibly detected with the novel PK-PET blot method.

Remarkably, much more neuritic pathology was detected on PK-PET blots of affected brain regions in LB diseases, such as the striatum (not shown) and SN pars compacta (Figure 2b), the hippocampal CA2/3 sector (Figure 2e), and the parahippocampal cortex (Figure 2h), compared with adjacent sections immunostained with αS using different antigen recovery methods, such as boiling in citrate buffer (Figure 2, c, f, and i), or standard PK or formic acid treatment (data not shown). All three standard immunohistochemical pretreatments revealed the same neuritic pathology (Figure 2, c, f, and i, and results not shown), which was less pronounced than the PK-PET blot staining. No PK-resistant αS was found in neurites of MSA cerebellum (Figure 2, j–l), indicating that αS misfolding in MSA is restricted to oligodendroglial cells.
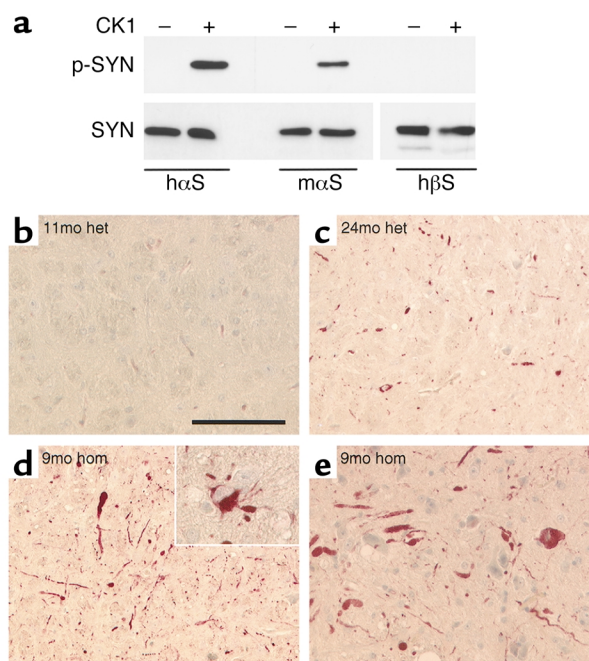
Thus, the PK-PET blot provides a highly sensitive method to detect specific pathology (PK resistance) of αS in the affected brain regions of α-synucleinopathy patients. Importantly, this novel method revealed that

neuritic α-synucleinopathy in patients with LB diseases is much more widespread and pronounced than expected from conventional αS immunostains.

Age- and gene dose–dependent neuronal α-synucleinopathy in αS transgenic mice. After having established PK-resistant αS as a novel in situ marker of LB diseases, we applied the PK-PET blot method to transgenic mice expressing the PD-associated mutant h[A30P]αS under control of the pan-neuronal Thy1 promoter (25). Heterozygous mouse lines 18 and 31 showed the same results, ruling out transgene integration artifacts. In 11-month-old heterozygous mice, no PK-resistant αS was detected (Figure 3a). Likewise, the nonamyloidogenic mouse βS was fully PK-labile (Figure 3b). However, as the heterozygous mice reached old age (24 months), PK-resistant αS became detectable in selected brain and SC regions. Although transgenic αS was highly expressed throughout the brain (Figure 3c), PK-resistant αS was detected in specific brain regions, including the zona incerta, the superior colliculus, the deep mesencephalic reticular field, the central gray, the pontine and medullary reticular formation, and the cerebellar nuclei (Figure 3d). Some of the affected brain regions in the

Figure 5
Pathological αS hyperphosphorylation in transgenic mice. (**a**) Human αS, mouse αS, and human βS were incubated without (–) or with (+) casein kinase 1 (CK1), and 20 ng synuclein aliquots were Western-probed with phosphospecific anti-αS (p-SYN, upper panel), MC42 anti-αS, and 6485 anti-βS, respectively (SYN, lower panels). (**b**–**e**) Immunohistochemistry with phosphospecific anti-αS of the pontine reticular field (**b**–**d**) and ventral horn of the SC (**e**) from heterozygous mice aged 11 months (**b**) and 24 months (**c**) as well as from a homozygous mouse aged 9 months (**d** and **e**). Inset in **d** highlights phospho-αS–containing neuronal cytosolic inclusions and neuritic swellings. Scale bar, 100 μm in **b**–**e**, 50 μm in inset.

transgenic mice have been implicated in PD (37). However, the striatum and the SN did not display PK-resistant transgenic αS (Figure 3d), most likely because the Thy1 promoter did not mediate high enough levels of transgenic αS expression in the SN (Figure 3c).

The same pathology developed in homozygous mice (Figure 3e), but approximately 1 year earlier than in heterozygotes. The accelerated development of pathology in the homozygous animals is probably due to higher expression levels. The transgenic αS levels in cytosolic fractions from homozygous mice (6.75 ± 0.55 ng/μg; n = 3) were significantly higher than in heterozygotes (1.69 ± 0.31 ng/μg; n = 3) (26).

A high density of PK-resistant αS was also detectable in the SC, particularly in the ventral horn and intermediate areas of the gray matter as well as in the white matter tracts (Figure 3f). Higher magnification of transgenic mouse PK-PET blots revealed that only a few neurites and cell bodies contained PK-resistant αS in the cortex (Figure 3g), whereas numerous LB-like structures as well as abundant neuritic profiles were detected in the brainstem (Figure 3h).

In the same brain regions that displayed PK-resistant αS, (Thy1)-αS mice showed further diagnostic features of human LB diseases. Argyrophilic profiles resembling LNs (Figure 4a) and, to a lesser extent, intraneuronal cytoplasmic inclusions reminiscent of LBs (Figure 4b) were observed upon Gallyas silver staining. The Campbell-Switzer method yielded the same results (not shown). The inclusions also showed intense TS labeling (Figure 4, c and d), indicating that the lesions contain structural elements with crossed β-pleated sheet conformations. At the ultrastructural level, the characteristic 9- to 12-nm filaments (38) were visible in the transgenic mouse brain inclusions (Figure 4, e and f), but not in presymptomatic mice or littermates (results not shown). Such electron-dense inclusions were typically well circumscribed, and often organelles (e.g., mitochondria) were entrapped in them.

The pathological hyperphosphorylation state of αS was assessed in the transgenic mice. Although the antiserum recognized in vitro–phosphorylated mouse αS as well as in vitro–phosphorylated human (transgenic) αS (Figure 5a), there was no immunoreactivity in nontransgenic mice (not shown), or in presymptomatic (Thy1)-αS mice (Figure 5b). With increasing age, however, heterozygous (Thy1)-αS mice showed somal and neuritic deposits of hyperphosphorylated αS (Figure 5c) concomitant with the aggravation of pathology described above. Furthermore, the phosphospecific anti-αS visualized severe pathology in symptomatic homozygous (Thy1)-αS mice (Figure 5, d and e). Inclusions containing hyperphosphorylated αS were observed in neuronal cytosol, and massively swollen neurites were abundant in the affected brain and SC regions described above.

Pathological modification of αS was further substantiated by the occurrence of dystrophic neurites and LB-like inclusions that reacted with two different mAb's raised against oxidized αS (30) (Figure 6, a and b). In contrast, sections from age-matched control mice were not stained with these pathological αS antibodies. Moreover, an antibody against nitrated αS (16, 30) also specifically reacted with sections of transgenic mouse brain (not shown). Furthermore, a subset of the LB-like inclusions and dystrophic neurites described above was immunoreactive for ubiquitin (Figure 6, c and d). The most severely affected brain and SC regions showed areas of intense astrogliosis (Figure 6e) indicative of ongoing neurodegeneration. However, comparison of SC sections from motor-impaired mice with those from littermates revealed no obvious loss of spinal motor neurons (Figure 6, g and h).

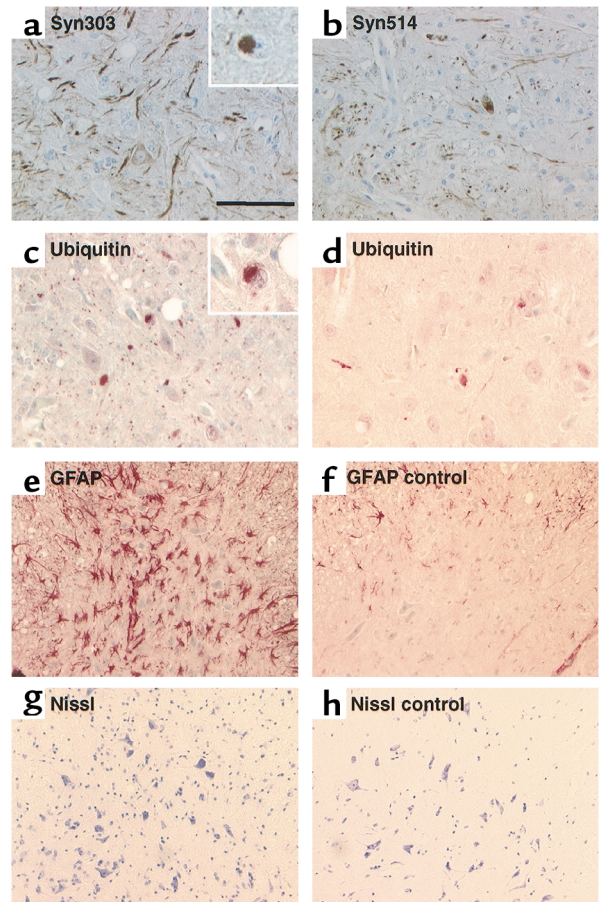The effects of αS expression on neurotransmitter content in aged transgenic mice were evaluated. In

Figure 6
Pathology in severely affected transgenic mouse brain regions. (**a** and **b**) Antibodies Syn303 (**a**) and Syn514 (**b**) against oxidatively modified αS stained numerous pathological neuritic profiles and occasional LB-like neuronal inclusions, one of which is magnified in the inset in **a**. (**c** and **d**) Anti-ubiquitin immunostaining showed some neuritic and cell body inclusions (inset in **c**). **a–c** are from the pontine reticular nuclei, and **d** is from the ventral horn of the SC. (**e** and **f**) Immunostaining of glial fibrillary acidic protein (GFAP) revealed prominent astrocytic gliosis in the most affected regions (here the ventral horn of the SC) in a motor-impaired homozygous (Thy1)-αS mouse (**e**) compared with a nontransgenic control mouse (**f**). (**g** and **h**) Nissl staining of the identical area of ventral horn revealed numerous motor spinal neurons in transgenic (**g**) and control (**h**) mice. Scale bar, 100 μm in **a–d**, 50 μm in inserts in **a** and **c**, 200 μm in **e–h**.

Table 1
Tissue content of dopamine, noradrenaline, serotonin, and metabolites in the striatum and frontal cortex of 8-month-old wild-type and homozygous (Thy1)-h[A30P]αS mice

Tissue content	Striatum		Frontal cortex	
(ng/g)	Wild-type	Transgenic mice	Wild-type	Transgenic mice
		Male mice		
Dopamine	9,839 ± 486	10,221 ± 711	55 ± 3	55 ± 2
DOPAC	995 ± 23	973 ± 55	32 ± 1	27 ± 1
HVA	1,058 ± 38	1,181 ± 55	82 ± 3	79 ± 3
Noradrenaline	444 ± 52	435 ± 44	532 ± 11	529 ± 10
Serotonin	1,895 ± 51	1,697 ± 51[A]	565 ± 17	693 ± 17[B]
5-HIAA	466 ± 20	396 ± 12[B]	142 ± 6	119 ± 6[A]
		Female mice		
Dopamine	12,140 ± 617	12,423 ± 571	59 ± 2	57 ± 2
DOPAC	1,175 ± 77	1,083 ± 48	33 ± 2.4	36 ± 2
HVA	1,210 ± 60	1,187 ± 42	79 ± 4	88 ± 6
Noradrenaline	253 ± 31	281 ± 24	508 ± 7	520 ± 10
Serotonin	1,904 ± 74	1,954 ± 55	642 ± 10	700 ± 18[A]
5-HIAA	416 ± 23	635 ± 28[B]	150 ± 10	162 ± 6

Data are presented as mean ± SE for wild-type (males, $n = 12$; females, $n = 9$) and homozygous (Thy1)-h[A30P]αS mice (males, $n = 11$; females, $n = 12$).
[A]$P < 0.05$, [B]$P < 0.01$; two-tailed t test. DOPAC, 3,4-dihydroxyphenylacetic acid; HVA, homovanillic acid; 5-HIAA, 5-hydroxyindoleacetic acid.

striatum and cortex of 2-year-old heterozygous mice, there was no effect on the striatal and cortical content of dopamine, noradrenaline, and serotonin. Only a small increase of the dopamine metabolite 3,4-dihydroxyphenylacetic acid and of the serotonin metabolite 5-hydroxyindoleacetic acid (5-HIAA) was observed in the striatum (data not shown). Next, we analyzed striatum and cortex of 8-month-old homozygous mice. In this cohort, the females were beginning to show impaired locomotor performance on the accelerated Rotorod (mean best performance out of three: 190.8 ± 13.9 seconds for transgenic females, 232.2 ± 7.7 seconds for control females). Still, we could not detect any differences in DA and its metabolites. There were, however, some small effects on serotonin and 5-HIAA (Table 1). Thus, synthesis and metabolism of dopamine were not affected, but some minor effect on the serotoninergic system was found in 8-month-old homozygous (Thy1)-h[A30P]αS mice.

Homozygous (Thy1)-h[A30P]αS mice further deteriorated in locomotor performance within the first year of life ($n = 13$). Initially the mice had an unsteady gait and a weakening of the extremities, progressing from the hind limbs to the forelimbs. Tail posture became abnormal, and tail movements were jerky. The end-stage phenotype was characterized by a hunchback posture and spastic paralysis of the hind limbs. Eventually the mice lost the capability to stand and reach the nutrition distributors but could be maintained for a few days by bottom feeding. The same phenotype was recently described for aged homozygous (PrP)-h[A53T]αS mice (39). Hind-limb clasping as previously observed upon overexpression of, for example, tau (40, 41) was not typical for αS transgenic mice, suggesting that αS expression in transgenic mice causes a specific locomotor phenotype.

Discussion
PK resistance is a salient feature of the misfolded proteins relevant to prion diseases and Alzheimer disease (20). By analogy, the PD gene product αS formed PK-resistant fibrils, in contrast to the nonamyloidogenic βS that lacks the critical stretch of amino acids in the NAC domain, consistent with previous reports (17–19). To elucidate the topology of αS within fibrils, an epitope-mapping study of PK-digested αS aggregates was undertaken. Using low concentrations of PK, we found truncated αS species that were detectable with antibodies against C-terminal epitopes. Higher concentrations of PK were necessary to produce the core NAC fragments (18, 19). Thus, the extreme N-terminus of αS in aggregates appears to be more accessible to PK than the C-terminus, which is more accessible than the core NAC fragments. This is in accord with a very recent immunoelectron-microscopic study, in which antibodies against both termini labeled αS fibrils before, but not after, PK treatment (19). Polyclonal antibody TI17 against amino acids 1–10 of αS also labeled the fibril sides (13). However, other N-terminal antibodies labeled αS fibrils less efficiently (17, 42), and polyclonal PER1 anti-αS(11-34) labeled only one end of fibrils isolated from DLB brain (43). It cannot be excluded that immunogold–electron microscopy sample preparation differentially affects accessibility of these antibodies. Limited PK digestion is advantageous because it allows refined epitope mapping of native αS fibrils in aqueous solution.

Very recently, PK resistance was described for αS fibrils isolated from MSA brain (19). Here we demonstrate the same property for αS fibrils from a neuronal α-synucleinopathy, namely DLB. The PK resistance of aggregated αS enabled us to develop a method to specifically detect pathologically misfolded αS in situ.

We digested PK-PET blots much more harshly (overnight at 55°C) than usual for epitope retrieval (10 minutes at 37°C) (44), probably removing most of the physiologically folded αS. The strong, normal αS staining in hippocampal and cortical neuropil may mask the massive neuritic αS pathology unveiled on PK-PET blots (Figure 2). PK-resistant αS was detected in the brain regions most affected by a given α-synucleinopathy, namely PD SN and striatum, as well as hippocampus and cortex of DLB and NBIA1 patients. Thus, neuritic αS pathology appears to be more marked than previously thought based on the immunostaining of LNs. In comparison, brainstem and cortical LBs are rare and may not account entirely for the loss of locomotor control in PD and dementia in DLB, respectively. In fact, there are some reports that LB-containing neurons appear morphologically healthier than adjacent ones (45). It is tempting to speculate that the neurites filled with PK-resistant αS mark a loss of neuronal connectivity that causes the symptoms of α-synucleinopathy patients.

PK resistance of αS also developed in the (Thy1)-h[A30P]αS transgenic mouse model. Pathological specificity was corroborated by close spatiotemporal correlation with standard markers of α-synucleinopathy, including silver staining, TS fluorescence, and electron-dense filaments. α-Synucleinopathy in these transgenic mice developed in a strictly age- and gene dose–dependent manner. Homozygous mice developed the same pathology over one year earlier. Moreover, a highly specific marker of α-synucleinopathy, namely S129 hyperphosphorylation, closely correlated with pathology in the transgenic mice. Some inclusions were ubiquitinated in severely affected regions where ongoing neurodegeneration was indicated by astrogliosis. Sensorimotor nuclei in the brainstem and the SC, but not the SN pars compacta, were predominantly affected, probably accounting for the locomotor phenotype.

The regional specificity of age-dependent α-synucleinopathy in (Thy1)-h[A30P]αS mice is remarkable. Despite robust expression of transgenic αS in the cortex and hippocampus, only scarce PK-resistant neurites and cell bodies were observed in these mouse brain regions. In contrast, the zona incerta, the deep mesencephalic and pontine nuclei, and reticular formation of the brainstem accumulated misfolded αS and eventually showed signs of neurodegeneration. Interestingly, the predilection sites of α-synucleinopathy in old (Thy1)-h[A30P]αS transgenic mice overlapped with the sites of earliest α-synucleinopathy in humans (37), most notably in the pontine and medullary reticular zones. In the affected neurons, a balance of pro-aggregative and anti-aggregative factors may be shifted to permit αS fibrillation. Regional differences of expression levels of the anti-aggregative βS (28) may predispose hindbrain neurons for α-synucleinopathy. In fact, patients with LB diseases were reported to express two- to threefold more αS and less βS mRNA than controls (46). Thus, the αS/βS ratio in neuronal cytosol may be a critical determinant of αS aggregation.

A second factor promoting αS fibril formation may be phosphorylation at S129 (12). Casein kinases and G protein–coupled receptor kinases are capable of specifically phosphorylating αS at this position (11, 47), but the (patho)physiologically relevant kinases have not been identified in brain. αS is hyperphosphorylated at S129 in pathological lesions, and in αS transgenic mice hyperphosphorylation correlated with pathology. Symptomatic, but not asymptomatic, strains of (PDGFβ)-h[wt]αS mice were immunoreactive for phospho-αS (12). In our (Thy1)-h[A30P]αS mice, hyperphosphorylation of αS became detectable in a strictly age- and gene dose–dependent manner, concomitant with the development of argyrophilic and TS-positive inclusions.

Unlike in human LB diseases, the SN of αS transgenic mice was relatively spared from pathology. In the case of (Thy1)-αS mice, this may be simply due to the fact that the Thy1 cassette does not express transgenes at high levels in the SN. Nevertheless, Thy1-controlled overexpression of αS led to neuropathology and gliosis, indicating that α-synucleinopathy causes neurodegenerative events and is not an epiphenomenon of LB diseases. Specifically, relatively early-onset and rapid degeneration of motor neurons in the SC, accompanied by gliosis and occasional ubiquitin staining, was reported for (Thy1)-h[A53T]αS mice (24). The degeneration of neuromuscular junctions and premature death of these animals precluded an aging study as reported here. In the present study, we show that a similar phenotype for (Thy1)-h[A30P]αS transgenic mice develops with late onset, and we unequivocally demonstrate that the αS deposits were highly similar to human LBs and LNs, as evidenced by (a) PK-PET blotting, (b) silver staining, (c) TS staining, (d) electron microscopy, and (e) immunoreactivity with antibodies specific for pathologically modified αS.

While this manuscript describing the phenotype of (Thy1)-h[A30P]αS mice was under consideration, two groups presented similar pathology and phenotype for (PrP)-h[A53T]αS mice (39, 48). Again, the brainstem and SC bore the brunt of αS pathology, whereas neocortex, hippocampus, and also SN were devoid of αS deposits (39). Dopamine levels were not determined and tyrosine hydroxylase activity was not quantified in these studies. Slight reductions in these DA parameters were reported for a highly overexpressing line of (PDGFβ)-h[wt]αS mice (23). Nonfibrillar, amorphic αS inclusions were occasionally found in the SN, but loss of DA neurons was not reported (23). Targeted expression of αS in DA neurons of the SN was achieved in transgenic mice using the tyrosine hydroxylase promoter (49, 50). These mice have been reported to diffusely accumulate αS in neuronal cell bodies and neurites, a phenotype also observed in young pan-neuronally expressing αS transgenic mice.

Thus, the nigral DA neurons were not particularly susceptible to α-synucleinopathy and neurodegeneration in the transgenic mouse models. It is likely that adaptive changes occur in the transgenic mice that express the transgenic αS from the first weeks of life on. When αS expression in rats was induced abruptly to extremely high levels upon infection with adeno-associated viral vectors, the nigrostriatal DA system was selectively damaged (51, 52). As in the transgenic mouse models, swollen neurites immunopositive for αS were frequently observed (51, 52). Granular cytosolic inclusions of αS were reported by Kirik et al. (52), but the amyloid nature of these pathological profiles was not (yet) demonstrated, and the inclusions could not be stained with anti-ubiquitin. The loss of DA neurons was not massive enough to cause drastic locomotor dysfunction, and the period of maximal damage around 1 month after infection was followed by some recovery of DA synapses 6 months after infection (52). Thus, viral transduction of nigral neurons in the rat allowed selective and acute damage of the nigrostriatal DA projections, whereas transgenic expression of αS in mice caused extranigral Lewy pathology and severe locomotor dysfunction in a progressive age-dependent manner. It will be interesting to determine whether viral superinfection of transgenic mice combines the advantages of both approaches to an improved animal model for PD.

The transgenic animal models suggest that αS expression alone causes an age-dependent development of Lewy pathology. The PD-associated αS mutation A53T enhanced the phenotype (24, 39, 48). Although Lee et al. reported no phenotype in their (PrP)-h[A30P]αS mice (48), this PD-associated mutation also caused Lewy pathology and neurodegeneration in mice (this study), rats (51), and *Drosophila* (21), demonstrating strong pathogenic effects of the A30P mutation. Furthermore, α-synucleinopathy ultimately led to deterioration of locomotor performance. Gliosis in the brainstem and SC was indicative of ongoing degeneration of neurons involved in movement control (refs. 24, 39, 48, and this study), but the neuronal population(s) that was actually lost remains to be identified in all transgenic mouse models.

Investigation of transgenic mouse models suggests a cascade of events that might occur in human patients as well. Earliest signs of α-synucleinopathy include a diffuse somal accumulation of detergent-insoluble αS in neurons (26). Upon aging, αS becomes PK-resistant, concomitant with the formation of typical αS fibrils. Ubiquitination was a secondary event seen at end stages of LB formation and is unlikely to cause αS fibrillization. Rather, hyperphosphorylation at S129 occurred as αS amyloid formed in vivo, possibly contributing to the age-dependent phenotype of (Thy1)-αS mice. In conclusion, αS transgenic mice may serve as a model system to study the molecular mechanisms underlying LB diseases and to validate anti-aggregation therapies.

1. Goedert, M. 2001. Alpha-synuclein and neurodegenerative diseases. *Nat. Rev. Neurosci.* **2**:492–501.
2. Abeliovich, A., et al. 2000. Mice lacking α-synuclein display functional deficits in the nigrostriatal dopamine system. *Neuron.* **25**:239–252.
3. Murphy, D.D., Rueter, S.M., Trojanowski, J.Q., and Lee, V.M.-Y. 2000. Synucleins are developmentally expressed, and α-synuclein regulates the size of the presynaptic vesicular pool in primary hippocampal neurons. *J. Neurosci.* **20**:3214–3220.
4. Polymeropoulos, M.H., et al. 1997. Mutation in the α-synuclein gene identified in families with Parkinson's disease. *Science.* **276**:2045–2047.
5. Krüger, R., et al. 1998. Ala30Pro mutation in the gene encoding α-synuclein in Parkinson's disease. *Nat. Genet.* **18**:106–108.
6. Spillantini, M.G., et al. 1997. α-Synuclein in Lewy bodies. *Nature.* **388**:839–840.
7. Takeda, A., et al. 1998. Abnormal accumulation of NACP/α-synuclein in neurodegenerative disorders. *Am. J. Pathol.* **152**:367–372.
8. Arawaka, S., Saito, Y., Murayama, S., and Mori, H. 1998. Lewy body in neurodegeneration with brain iron accumulation type 1 is immunoreactive for α-synuclein. *Neurology.* **51**:887–889.
9. Arai, K., Kato, N., Kashiwado, K., and Hattori, T. 2000. Pure autonomic failure in association with human α-synucleinopathy. *Neurosci. Lett.* **296**:171–173.
10. Dickson, D.W., Lin, W., Liu, W.K., and Yen, S.H. 1999. Multiple system atrophy: a sporadic synucleinopathy. *Brain Pathol.* **9**:721–732.
11. Okochi, M., et al. 2000. Constitutive phosphorylation of the Parkinson's disease associated α-synuclein. *J. Biol. Chem.* **275**:390–397.
12. Fujiwara, H., et al. 2002. α-Synuclein is phosphorylated in synucleinopathy lesions. *Nat. Cell Biol.* **4**:160–164.
13. Conway, K.A., Harper, J.D., and Lansbury, P.T. 1998. Accelerated in vitro fibril formation by a mutant α-synuclein linked to early-onset Parkinson disease. *Nat. Med.* **4**:1318–1320.
14. Narhi, L., et al. 1999. Both familial Parkinson's disease mutations accelerate α-synuclein aggregation. *J. Biol. Chem.* **274**:9843–9846.
15. Hashimoto, M., et al. 1999. Oxidative stress induces amyloid-like aggregate formation of NACP/α-synuclein in vitro. *Neuroreport.* **10**:717–721.
16. Souza, J.M., Giasson, B.I., Chen, Q., Lee, V.M.-Y., and Ischiropoulos, H. 2000. Dityrosine cross-linking promotes formation of stable α-synuclein polymers. Implication of nitrative and oxidative stress in the pathogenesis of neurodegenerative synucleinopathies. *J. Biol. Chem.* **275**:18344–18349.
17. Conway, K.A., Harper, J.D., and Lansbury, P.T., Jr. 2000. Fibrils formed in vitro from α-synuclein and two mutant forms linked to Parkinson's disease are typical amyloid. *Biochemistry.* **39**:2552–2563.
18. Giasson, B.I., Murray, I.V.J., Trojanowski, J.Q., and Lee, V.M.-Y. 2001. A hydrophobic stretch of 12 amino acid residues in the middle of α-synuclein is essential for filament assembly. *J. Biol. Chem.* **276**:2380–2386.
19. Miake, H., Mizusawa, H., Iwatsubo, T., and Hasegawa, M. 2002. Biochemical characterization of the core structure of α-synuclein filaments. *J. Biol. Chem.* **277**:19213–19219.
20. Forloni, G. 1996. Neurotoxicity of β-amyloid and prion peptides. *Curr. Opin. Neurol.* **9**:492–500.
21. Feany, M.B., and Bender, W.W. 2000. A *Drosophila* model of Parkinson's disease. *Nature.* **404**:394–398.
22. Auluck, P.K., Chan, H.Y.E., Trojanowski, J.Q., Lee, V.M.-Y., and Bonini, N.M. 2002. Chaperone suppression of α-synuclein toxicity in a *Drosophila* model for Parkinson's disease. *Science.* **295**:865–868.
23. Masliah, E., et al. 2000. Dopaminergic loss and inclusion body formation in α-synuclein mice: implications for neurodegenerative disorders. *Science.* **287**:1265–1269.
24. van der Putten, H., et al. 2000. Neuropathology in mice expressing human α-synuclein. *J. Neurosci.* **20**:6021–6029.
25. Kahle, P.J., et al. 2000. Subcellular localization of wild-type and Parkinson's disease-associated mutant α-synuclein in human and transgenic mouse brain. *J. Neurosci.* **20**:6365–6373.
26. Kahle, P.J., et al. 2001. Selective insolubility of α-synuclein in human Lewy body diseases is recapitulated in a transgenic mouse model. *Am. J. Pathol.* **159**:2215–2225.
27. Masliah, E., et al. 2001. β-Amyloid peptides enhance α-synuclein accumulation and neuronal deficits in a transgenic mouse model linking Alzheimer's disease and Parkinson's disease. *Proc. Natl. Acad. Sci. USA.* **98**:12245–12250.

28. Hashimoto, M., Rockenstein, E., Mante, M., Mallory, M., and Masliah, E. 2001. β-Synuclein inhibits α-synuclein aggregation. A possible role as an anti-Parkinsonian factor. *Neuron.* **32**:213–223.

29. Trenkwalder, C., et al. 1995. Starnberg trial on epidemiology of Parkinsonism and hypertension in the elderly. Prevalence of Parkinson's disease and related disorders assessed by a door-to-door survey of inhabitants older than 65 years. *Arch. Neurol.* **52**:1017–1022.

30. Giasson, B.I., et al. 2000. Oxidative damage linked to neurodegeneration by selective α-synuclein nitration in synucleinopathy lesions. *Science.* **290**:985–989.

31. Schulz-Schaeffer, W.J., et al. 2000. The paraffin-embedded tissue blot detects PrP^Sc early in the incubation time in prion diseases. *Am. J. Pathol.* **156**:51–56.

32. Specht, C.G., and Schoepfer, R. 2001. Deletion of the α-synuclein locus in a subpopulation of C57BL/6J inbred mice. *BMC Neurosci.* **2**:11.

33. Da Prada, M., et al. 1988. Neurochemical profile of moclobemide, a short-acting and reversible inhibitor of monoamine oxidase type A. *J. Pharmacol. Exp. Ther.* **248**:400–414.

34. Taraboulos, A., et al. 1992. Regional mapping of prion proteins in brain. *Proc. Natl. Acad. Sci. USA.* **89**:7620–7624.

35. McKeith, I.G., et al. 1996. Consensus guidelines for the clinical and pathologic diagnosis of dementia with Lewy bodies (DLB): report of the consortium on DLB international workshop. *Neurology.* **47**:1113–1124.

36. Neumann, M., et al. 2000. α-Synuclein accumulation in a case of neurodegeneration with brain iron accumulation type 1 (NBIA-1, formerly Hallervorden-Spatz syndrome) with widespread cortical and brainstem-type Lewy bodies. *Acta Neuropathol.* **100**:568–574.

37. Del Tredici, K., Rüb, U., de Vos, R.A.I., Bohl, J.R.E., and Braak, H. 2002. Where does Parkinson disease pathology begin in the brain? *J. Neuropathol. Exp. Neurol.* **61**:413–426.

38. Arima, K., et al. 1998. Immunoelectron-microscopic demonstration of NACP/α-synuclein-epitopes on the filamentous component of Lewy bodies in Parkinson's disease and in dementia with Lewy bodies. *Brain Res.* **808**:93–100.

39. Giasson, B.I., et al. 2002. Neuronal α-synucleinopathy with severe movement disorder in mice expressing A53T human α-synuclein. *Neuron.* **34**:521–533.

40. Ishihara, T., et al. 1999. Age-dependent emergence and progression of a tauopathy in transgenic mice overexpressing the shortest human tau isoform. *Neuron.* **24**:751–762.

41. Lewis, J., et al. 2000. Neurofibrillary tangles, amyotrophy and progressive motor disturbance in mice expressing mutant (P301L) tau protein. *Nat. Genet.* **25**:402–405.

42. Giasson, B.I., Uryu, K., Trojanowski, J.Q., and Lee, V.M.-Y. 1999. Mutant and wild type human α-synucleins assemble into elongated filaments with distinct morphologies in vitro. *J. Biol. Chem.* **274**:7619–7622.

43. Spillantini, M.G., Crowther, R.A., Jakes, R., Hasegawa, M., and Goedert, M. 1998. α-Synuclein in filamentous inclusions of Lewy bodies from Parkinson's disease and dementia with Lewy bodies. *Proc. Natl. Acad. Sci. USA.* **95**:6469–6473.

44. Takeda, A., et al. 1998. Abnormal distribution of the non-Aβ component of Alzheimer's disease amyloid precursor/α-synuclein in Lewy body disease as revealed by proteinase K and formic acid pretreatment. *Lab. Invest.* **78**:1169–1177.

45. Tompkins, M.M., and Hill, W.D. 1997. Contribution of somal Lewy bodies to neuronal death. *Brain Res.* **775**:24–29.

46. Rockenstein, E., et al. 2001. Altered expression of the synuclein family mRNA in Lewy body and Alzheimer's disease. *Brain Res.* **914**:48–56.

47. Pronin, A.N., Morris, A.J., Surguchov, A., and Benovic, J.L. 2000. Synucleins are a novel class of substrates for G protein-coupled receptor kinases. *J. Biol. Chem.* **275**:26515–26522.

48. Lee, M.K., et al. 2002. Human α-synuclein-harboring familial Parkinson's disease-linked Ala-53 → Thr mutation causes neurodegenerative disease with α-synuclein aggregation in transgenic mice. *Proc. Natl. Acad. Sci. USA.* **99**:8968–8973.

49. Rathke-Hartlieb, S., et al. 2001. Sensitivity to MPTP is not increased in Parkinson's disease-associated mutant α-synuclein transgenic mice. *J. Neurochem.* **77**:1181–1184.

50. Matsuoka, Y., et al. 2001. Lack of nigral pathology in transgenic mice expressing human α-synuclein driven by the tyrosine hydroxylase promoter. *Neurobiol. Dis.* **8**:535–539.

51. Klein, R.L., King, M.A., Hamby, M.E., and Meyer, E.M. 2002. Dopaminergic cell loss induced by human A30P α-synuclein gene transfer to the rat substantia nigra. *Hum. Gene Ther.* **13**:605–612.

52. Kirik, D., et al. 2002. Parkinson-like neurodegeneration induced by targeted overexpression of α-synuclein in the nigrostriatal system. *J. Neurosci.* **22**:2780–2791.